



AFRL-RZ-WP-TR-2010-2040

DESIGN OF AERODYNAMICALLY LOADED WAKE GENERATORS

Steven L. Puterbaugh and David Car

**Fan and Compressor Branch
Turbine Engine Division**

**JANUARY 2010
Interim Report**

Approved for public release; distribution unlimited.

See additional restrictions described on inside pages

STINFO COPY

**AIR FORCE RESEARCH LABORATORY
PROPULSION DIRECTORATE
WRIGHT-PATTERSON AIR FORCE BASE, OH 45433-7251
AIR FORCE MATERIEL COMMAND
UNITED STATES AIR FORCE**

NOTICE AND SIGNATURE PAGE

Using Government drawings, specifications, or other data included in this document for any purpose other than Government procurement does not in any way obligate the U.S. Government. The fact that the Government formulated or supplied the drawings, specifications, or other data does not license the holder or any other person or corporation; or convey any rights or permission to manufacture, use, or sell any patented invention that may relate to them.

This report was cleared for public release by the USAF 88th Air Base Wing (88 ABW) Public Affairs (AFRL/PA) Office and is available to the general public, including foreign nationals. Copies may be obtained from the Defense Technical Information Center (DTIC) (<http://www.dtic.mil>).

AFRL-RZ-WP-TR-2010-2040 HAS BEEN REVIEWED AND IS APPROVED FOR PUBLICATION IN ACCORDANCE WITH THE ASSIGNED DISTRIBUTION STATEMENT.

*//Signature//

STEVEN L. PUTERBAUGH, Work Unit Mgr
Fan and Compressor Branch
Turbine Engine Division

//Signature//

WILLIAM W. COPENHAVER , Acting Chief
Fan and Compressor Branch
Turbine Engine Division

//Signature//

JEFFREY M. STRICKER
Turbine Engine Division
Propulsion Directorate

This report is published in the interest of scientific and technical information exchange, and its publication does not constitute the Government's approval or disapproval of its ideas or findings.

*Disseminated copies will show “//Signature//” stamped or typed above the signature blocks.

REPORT DOCUMENTATION PAGE				<i>Form Approved OMB No. 0704-0188</i>	
The public reporting burden for this collection of information is estimated to average 1 hour per response, including the time for reviewing instructions, searching existing data sources, gathering and maintaining the data needed, and completing and reviewing the collection of information. Send comments regarding this burden estimate or any other aspect of this collection of information, including suggestions for reducing this burden, to Department of Defense, Washington Headquarters Services, Directorate for Information Operations and Reports (0704-0188), 1215 Jefferson Davis Highway, Suite 1204, Arlington, VA 22202-4302. Respondents should be aware that notwithstanding any other provision of law, no person shall be subject to any penalty for failing to comply with a collection of information if it does not display a currently valid OMB control number. PLEASE DO NOT RETURN YOUR FORM TO THE ABOVE ADDRESS.					
1. REPORT DATE (DD-MM-YY) January 2010		2. REPORT TYPE Interim		3. DATES COVERED (From - To) 01 March 2004 – 29 October 2004	
4. TITLE AND SUBTITLE DESIGN OF AERODYNAMICALLY LOADED WAKE GENERATORS				5a. CONTRACT NUMBER In-house	
				5b. GRANT NUMBER	
				5c. PROGRAM ELEMENT NUMBER 62203F	
6. AUTHOR(S) Steven L. Puterbaugh and David Car				5d. PROJECT NUMBER 3066	
				5e. TASK NUMBER 04	
				5f. WORK UNIT NUMBER 306604TK	
7. PERFORMING ORGANIZATION NAME(S) AND ADDRESS(ES) Fan Compressor Branch (AFRL/PRTF) Turbine Engine Division Air Force Research Laboratory, Propulsion Directorate Wright-Patterson Air Force Base, OH 45433-7251 Air Force Materiel Command, United States Air Force				8. PERFORMING ORGANIZATION REPORT NUMBER AFRL-RZ-WP-TR-2010-2040	
9. SPONSORING/MONITORING AGENCY NAME(S) AND ADDRESS(ES) Air Force Research Laboratory Propulsion Directorate Wright-Patterson Air Force Base, OH 45433-7251 Air Force Materiel Command United States Air Force				10. SPONSORING/MONITORING AGENCY ACRONYM(S) AFRL/RZTF	
				11. SPONSORING/MONITORING AGENCY REPORT NUMBER(S) AFRL-RZ-WP-TR-2010-2040	
12. DISTRIBUTION/AVAILABILITY STATEMENT Approved for public release; distribution unlimited.					
13. SUPPLEMENTARY NOTES Paper contains color. PA Case Number: 88ABW-2010-0491; Clearance Date: 05 Feb 2010. Research on this report was completed in 2004.					
14. ABSTRACT This report documents the design of a set of vane rows that were used to simulate the stator-exit conditions of a moderately loaded fan stage. These vanes were intended to be used in detailed characterization of the intra-blade flow field existing between the wake generator and the rotor in the Stage Matching Investigation (Fan Configuration) test article. This is in support of the Blade Row Interaction Task under the Innovative Aero Approaches to High Stage Loading RZT High Impact Technologies (HIT) in-house research program.					
15. SUBJECT TERMS flow control, stator diffusion, compression, turbine engine					
16. SECURITY CLASSIFICATION OF:			17. LIMITATION OF ABSTRACT: SAR	18. NUMBER OF PAGES 32	19a. NAME OF RESPONSIBLE PERSON (Monitor) Steven L. Puterbaugh 19b. TELEPHONE NUMBER (Include Area Code) N/A
a. REPORT Unclassified	b. ABSTRACT Unclassified	c. THIS PAGE Unclassified			

Table of Contents

<u>Section</u>	<u>Page</u>
List of Figures	iv
List of Tables	iv
Preface.....	v
Acknowledgement	vi
1. Summary	1
2. Introduction.....	2
3. Methods, Assumptions, and Procedures	3
3.1. Design Approach	3
3.1.1. Original Design Approach	3
3.1.2. Final Design Approach	5
4. Results and Discussion	6
4.1. Design Details	6
4.1.1. Swirler Section.....	7
4.1.2. Stator Section	10
5. Conclusions	17
References	18
Appendix A.....	19
LIST OF ACRONYMS, ABBREVIATIONS, AND SYMBOLS	21

List of Figures

Figure	Page
1. Design Cycle.....	3
2. Throughflow Model Computational Mesh Used in the Original Approach	4
3. Swirler Section Surface Traces.....	4
4. Stator Section Surface Traces	4
5. Stator Section Exit Mach Number	5
6. Rotor Inlet Relative Mach Number	5
7. Throughflow Model Computational Mesh Used in the Final Design Approach	5
8. Swirler Section Design Angular Momentum Distribution	7
9. Stator Section Design Angular Momentum Distribution.....	7
10. Swirler Section Airfoil Stack (Hub, Mid, and Tip Sections)	7
11. Multiple Views of the Swirler Section Vane	8
12. Swirler Vane Solidity	8
13. Flow Angle at the Swirler Trailing Edge Throughflow/CFD Comparision	9
14. Mach Number at the Swirler Trailing Edge Throughflow/CFD Comparison	9
15. Swirler Vane Loss Coefficient Distribution Obtained from the CFD Simulation	10
16. Swirler Vane Deviation Angle Distribution Throughflow/CFD Comparison	10
17. Swirler Vane Suction Side Near-Surface Flow Traces.....	10
18. Swirler Vane Pressure Side Near-Surface Flow Traces	10
19. Stator Section Endwall Vortex Trajectories	11
20. Stator Section Airfoil Stack (Hub, Mid, and Tip Sections)	12
21. Multiple Views of the Stator Section Vane	12
22. Spanwise Solidity Distribution for the Stator Vane Section.....	13
23. Spanwise Diffusion Factor Distribution for the Stator Vane Section	13
24. Stator Vane Section Inlet Mach Number Spanwise Distribution	13
25. Stator Vane Section Exit Mach Number Spanwise Distribution	13
26. Stator Section Incidence Angle Spanwise Distribution	14
27. Stator Section Inlet Flow Angle Spanwise Distribution	14
28. Stator Section Deviation Angle Spanwise Distribution.....	14
29. Stator Section Exit Flow Angle Spanwise Distribution.....	14
30. Stator Section Loss Coefficient Spanwise Distribution.....	15
31. Stator Section Pressure Side Near-Surface Flow Traces	15
32. Stator Section Suction Side Near-Surface Flow Traces	15
33. Rotor Relative Flow Angle Spanwise Distribution	16
34. Rotor Relative Mach Number Spanwise Distribution	16
35. Rotor Incidence Angle Distribution.....	16

List of Tables

Table	Page
1. Detailed Design Parameters.....	6
2. Stator Section Airfoil Thickness Distribution Parameters.....	11
A-1. NACA 65 Thickness Distribution.....	19

Preface

This report was prepared by Steven L. Puterbaugh and David Car of the Fan and Compressor Branch, Turbine Engine Division, Propulsion Directorate of the Air Force Research Labs. The work was executed in the period from March 2004 – October 2004.

This report represents a portion of the work conducted under Work Unit TK, Task 04, of Project 3066.

Acknowledgement

The authors gratefully acknowledge the contributions of Dr. Leroy Smith, consultant to General Electric Aircraft Engines, concerning suggested design parametrics and configuration features. The relevance of the configuration and the flexibility enabled by the design approach are due in large part to his contributions.

Design of Aerodynamically Loaded Wake Generators

1. Summary

This report documents the design of a set of vane rows that were used to simulate the stator-exit conditions of a moderately loaded fan stage. These vanes were intended to be used in detailed characterization of the intra-blade flow field existing between the wake generator and the rotor in the Stage Matching Investigation (Fan Configuration) test article. This is in support of the Blade Row Interaction Task under the Innovative Aero Approaches to High Stage Loading RZT High Impact Technologies (HIT) in-house research program.

2. Introduction

Previous CARL Blade Row Interaction work employed the Stage Matching Investigation (SMI) test article that utilized a set of uncambered “wake generators” to simulate the wakes of an upstream moderately loaded stator. The wake generator created the wakes through base drag via a rather thick profile and blunt trailing edge. This configuration was tested in the CARL facility at various wake generator-rotor spacings [1,2]. Detailed Particle Image Velocimetry (PIV) measurements revealed vortex shedding at the wake generator trailing edge that was locked to rotor blade passing frequency. Further, loss production was seen to increase due to an interaction between the rotor bow shock and the effective pressure surface flow field. Since the shape of the wake generator in the original work was not representative of stator airfoils that are typically employed in aero engines, it was important to determine whether the flow physics observed in the original work occurred for more typical airfoil geometry, specifically sections that contained camber and thinner trailing edges. The decision was therefore made to redesign the wake generators so that the aerodynamic and geometric characteristics more closely resembled typical practice. In order to employ an airfoil that contained camber and behaved like a realistic vane, the flow entering the vane was required to have some amount of swirl. Therefore two vane rows were designed. The first swirled the flow, the second removed the swirl and was used to simulate a stator vane row. These new blade row sets were to be the subject of a detailed investigation of the aerodynamic interaction between the stator section (second blade row) and the downstream rotor.

3. Methods, Assumptions, and Procedures

3.1. Design Approach

The computational tools used for the design included the USAF throughflow turbomachinery design code UD0300, and the NASA-developed computational fluid dynamics multi-blade row code APNASA. Additionally, in-house-developed utilities were used to make specific geometric modifications. The design cycle is depicted in Figure 1. There are two iterative design loops. The first, Phase I, includes big changes in flow path and design distributions and iterates between the throughflow and CFD calculations. The second, Phase II, includes relatively small changes in blade shape and iterates between blade modification utilities and CFD calculations.

In order to employ a loaded blade row to act as the wake generator, swirl must be imparted to the flow at some upstream location. The approach was to use 2 blade rows for the new wake generator configuration – the first acts as a swirler, the second as a de-swirler (or stator). The program was cost constrained and therefore sought to reutilize as much hardware as possible from the previous configuration. Therefore the following design constraints were applied: 1) The casing was retained, 2) the hub diameter upstream and downstream of the redesigned wake generator segment was retained, and 3) the axial extent of the new wake generator segment was limited to the length of the previous wake generator's flow path segment.

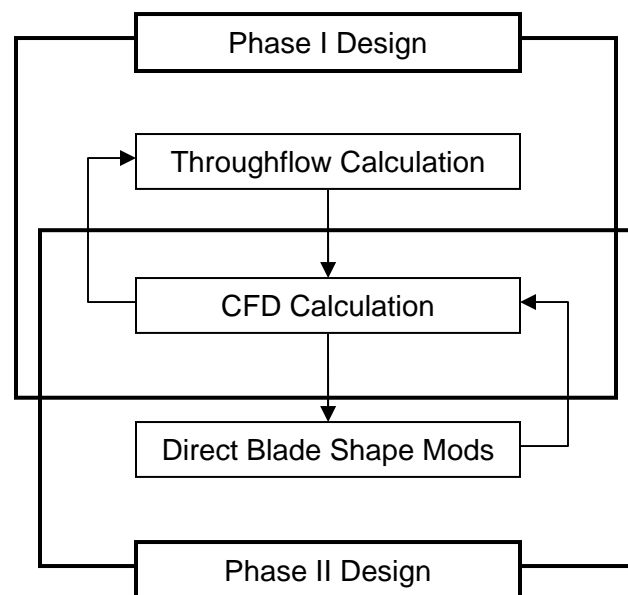


Figure 1 Design Cycle

3.1.1. Original Design Approach

The aerodynamic performance objectives originally included specifying the inlet Mach number, the inlet flow angle, and the exit flow angle for the stator section. The choice for inlet conditions was based on that typically found in a highly loaded stage, the Mach number was 0.8 and the inlet flow angle was 45°. The exit flow was required to be axial in order to match the original rotor design conditions.

The required flow angle - Mach number combination at a given flow rate uniquely specifies the annulus area at an axial plane, in this case at the stator section inlet. Since the case was to be retained, the hub flow path was modified. The starting point was determined by the relation

$$R_H = \sqrt{R_T^2 - \frac{\dot{m}}{\rho V \cos \alpha \pi}} \quad (1)$$

The resulting value of hub radius for the desired conditions was used to begin laying out the annulus profile at the swirler exit/stator inlet. Subsequent CFD analysis that more accurately predicted blockage was then to be used to adjust the hub radius to obtain the proper entrance conditions to the stator section.

The meridional flow path is shown in Figure 2.

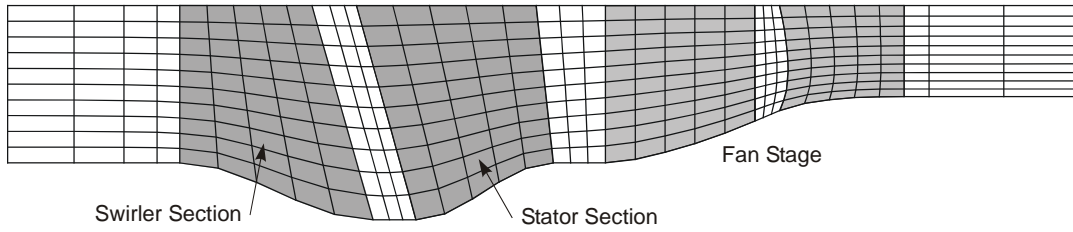


Figure 2 Throughflow Model Computational Mesh used in the Original Approach

CARL-typical blading thickness distributions using 3rd order curves were used for this initial design approach. APNASA was used to analyze the design. The flow field within the wake generators was fairly well behaved at this preliminary stage of design. The effect of secondary flow can be seen near the hub and tip in the swirler section suction surface traces in Figure 3 and near the hub in the stator section suction surface traces in Figure 4.

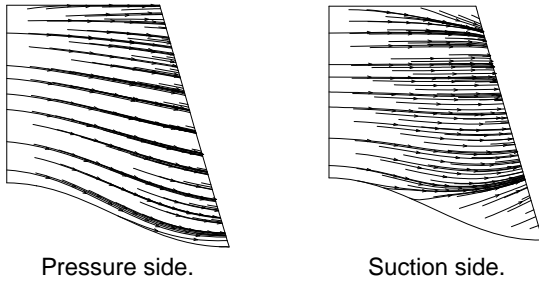


Figure 3 Swirler Section Surface Traces

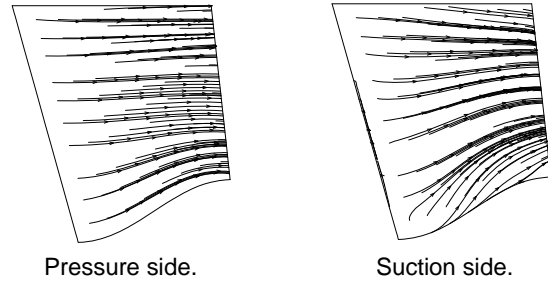


Figure 4 Stator Section Surface Traces

However, the severe hub curvature as the trailing edge is approached in the stator section results in a meridional acceleration in the flow and a non-uniform spanwise Mach number distribution as shown in Figure 5. The result is a poor match to the rotor inlet condition requirements, including driving the rotor to operate as fully supersonic as shown in Figure 6.

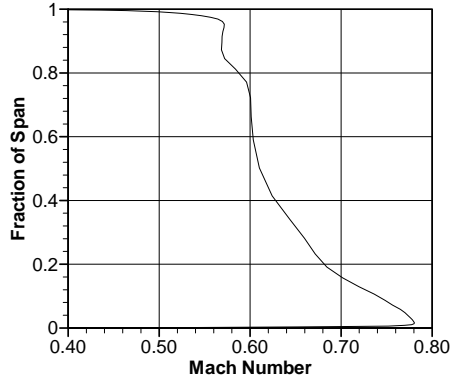


Figure 5 Stator Section Exit Mach Number

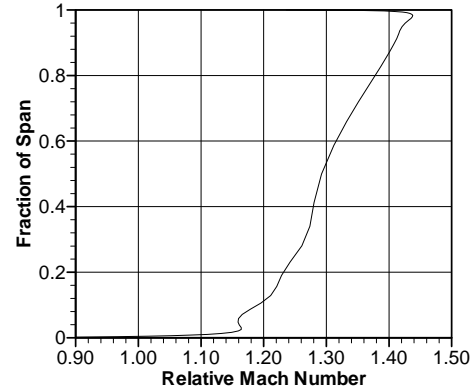


Figure 6 Rotor Inlet Relative Mach Number

3.1.2. Final Design Approach

Because of the high hub exit Mach numbers at the stator section exit, the decision was made to return to the cylindrical inner flowpath as shown in Figure 7 and accept the associated reduced flow angle at the stator section leading edge. The stator section inlet flow angle was reduced from 45° to 28.9° as a result of the reduced annulus area in this region relative to the original design approach. Since the outlet flow angle was fixed at 0° (axial) to maintain compatibility with the rotor, the turning through the stator section reduced from 45° to 28.9° as well. In order to maintain acceptable loading levels in the face of the reduced turning, the solidity was adjusted toward a target diffusion factor of 0.45.

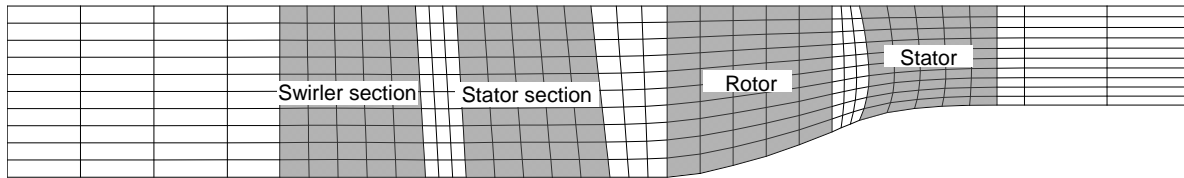


Figure 7 Throughflow Model Computational Mesh used in the Final Design Approach

The swirler section was designed to allow vane angle variation in order to change the loading on the stator section. Additionally, a NACA65 thickness distribution was used for the swirler section to minimize the wake depth and width. The throughflow code UD0300M was modified to generate a NACA65 series airfoil thickness distribution consistent with recommendations by Cumpsty [3]. Details of the implementation into UD0300M are included in Appendix A.

The stator section's airfoil sections were generated using cubic surface coordinate functions typical of CARL-designed airfoils. Further, the absolute value of airfoil thickness was driven by the need to insert laser illumination through the max thickness location for use with Particle Image Velocimetry measurements.

The aerodynamic phenomena under investigation are influenced by the proximity of the wake generator trailing edge and the rotor leading edge. Therefore, the meridional shape and position of the original wake generator trailing edge was retained in the new design.

4. Results and Discussion

4.1. Design Details

The blade row-specific detailed design parameters are shown in Table 1. The swirler section incidence of -2° was chosen to provide good performance over a $\pm 5^\circ$ range of vane resets. The vane count for each section was kept equal so that the relative location of the wake of the swirler section vanes would be the same for each stator section passage around the annulus. The specific choice of 32 vanes was made based on a combination of rotor modal response, PIV optical access, and multi-blade row numerical simulation considerations. The stator section incidence of 3° was chosen based on CARL design experience. Finally, the choice of stator section diffusion factor was made to keep the loading in the moderate-to-high range in order to assess the rotor's aerodynamic influence on a thick suction side boundary layer.

Table 1 Detailed Design Parameters

Flow Rate	34.46 lbm/sec
Specific Flow Rate	40.00 lbm/sec/ft ²
Swirler Section	
Incidence angle	-2°
Vane count	32
Stator Section	
Incidence angle	3°
Vane count	32
Inlet Mach number	0.8
Diffusion Factor	0.45
Discharge flow angle	0°

Further design constraints were applied based on mechanical design and fabrication requirements. The blade rows were to be mounted using multiple pins at the hub and tip. This required a minimum amount of vane material to be available to hold the pins. The pin size was based on loading requirements. Based on recommendations by the fabricator, a minimum airfoil thickness of 0.160" was required at the pinning locations. The locations were separated by a minimum of 40% chord to resist the moment on the airfoil about the stack axis caused by the aero loads.

The philosophy used to specify the streamwise loading distribution followed current design practice at the CARL. The approach is to move the loading as far forward as possible without causing leading edge separation. This approach reduces deviation and provides more accuracy in setting the cascade exit flow angle. Since the magnitude of flow angle change through the swirler section exceeds typical IGV design point requirements, a separate area distribution analysis was performed to make sure that a smooth, monotonic decrease in area was achieved via the streamwise blade angle distribution. The resulting distribution was consistent with the forward loading approach taken in the stator section as shown in Figures 8 and 9.

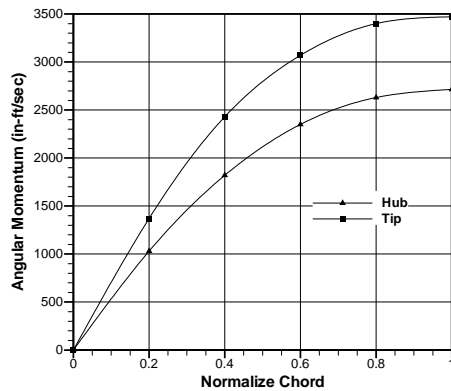


Figure 8 Swirler Section Design Angular Momentum Distribution

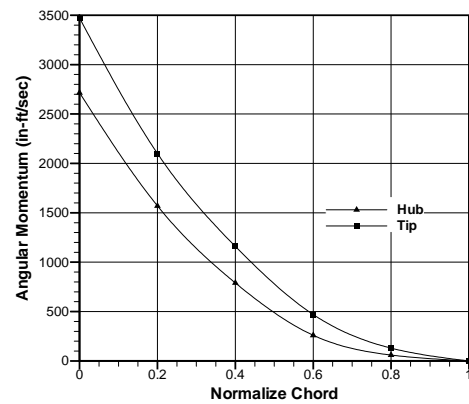


Figure 9 Stator Section Design Angular Momentum Distribution

4.1.1. Swirler Section

The intent of the swirler section was to impart the turning necessary for stator section inlet conditions with a minimum of loss (and associated wake width and depth). A NACA65 series thickness distribution was chosen for this purpose. A stacking line view of the swirler showing hub, mid, and tip streamsurface sections is shown in Figure 10. The max thickness for the outer 2 streamlines was set to 10% chord for attachment considerations. The max thickness at the remaining inboard sections was 8%. The leading edge radius is defined by the NACA65 thickness distribution whereas the trailing edge was specified as a constant 0.25% chord over the span. Multiple views of 3D renderings of the vane are shown in Figure 11. The view looking down the chord (middle) illustrates the fairing added at the hub and casing to allow for pin attachments at those locations.

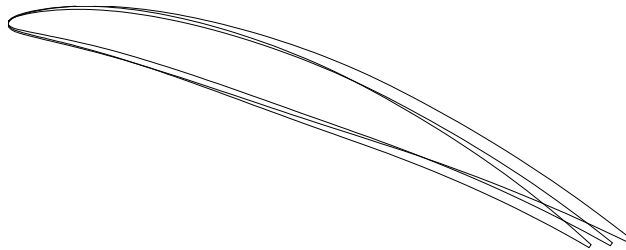


Figure 10 Swirler Section Airfoil Stack (Hub, Mid, and Tip Sections)



Figure 11 Multiple Views of the Swirler Section Vane

Since the flow through the swirler is accelerating, the solidity was not critical and resulted from requirements and constraints on other items. The axial length of the swirler/stator vane row set was limited by the inner and outer hardware rings used for the previous wake generators. The stator section solidity was manipulated directly to achieve the proper Diffusion Factor distribution (discussed later), leaving the remaining axial length less the gap between the vane rows to the swirler section. Further, the swirler vane count was required to be the same as the stator vane count to maintain consistent upstream/downstream vane wake relative positioning throughout the circumference. The resulting swirler vane spanwise solidity distribution is shown in Figure 12.

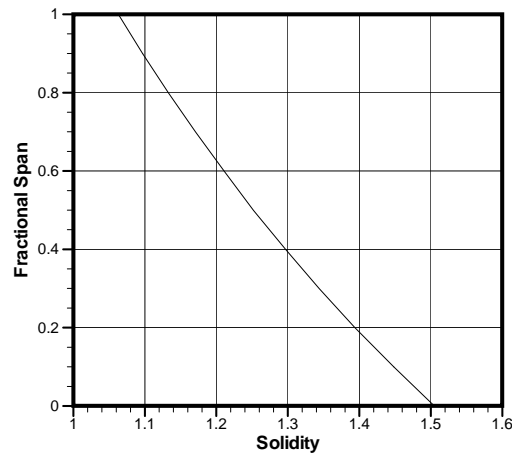


Figure 12 Swirler Vane Solidity

Many of the subsequent figures show a comparison between the design system (UD0300M throughflow model) values and those resulting from the CFD (APNASA) simulations. The CFD simulation results were mass averaged in the circumferential direction to provide the spanwise distributions shown. Differences between the two can be attributed to 3 dimensional flow and blockage effects captured by the simulation along with calculations of loss generating phenomena in the simulation versus loss modeling in the throughflow method. Throughout the design process, the CFD simulations were used as the final arbiter in modifications to blade shapes applied in the throughflow model.

In order to increase the experimental flexibility of the hardware to be built based on this design, it was determined to provide variable vane resets for the swirler section. This would allow the loading on the

stator section to be modified at a given flow rate, providing direct control over the suction side boundary layer thickness. To accommodate this feature, the swirler section was designed with a constant -2° incidence over the span.

The deflection, or turning, requirement through the swirler section was defined by the inlet conditions required by the stator section. A combination of the annulus shape constraint (cylindrical annulus), the stator section inlet Mach number constraint (0.8), and the specified flow rate drove the distribution of flow angle as seen in Figure 13. The resulting flow angle distribution centered around approximately 30° as opposed to the original specification of 45° . The expected overturning of the flow is clearly evident near the endwalls in the distributions generated by the CFD simulation.

The Mach number distribution at the swirler trailing edge is shown in Figure 14. Again, the endwall effect is seen which results primarily from the overturning seen previously. The increase in Mach number in the CFD simulation is due to blockage and loss calculated by the method.

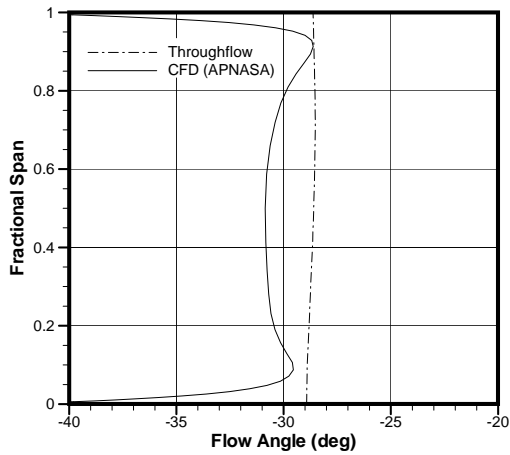


Figure 13 Flow Angle at the Swirler Trailing Edge Throughflow/CFD Comparison

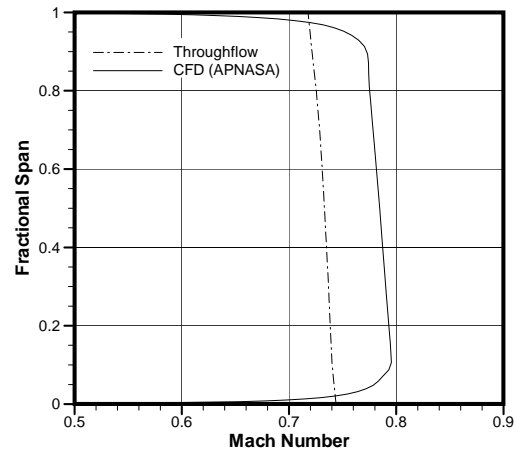


Figure 14 Mach Number at the Swirler Trailing Edge Throughflow/CFD Comparison

The loss coefficient calculated from the CFD simulation is shown in Figure 15. The loss coefficient is defined as the total pressure loss along a streamline normalized by the inlet dynamic head. For the CFD results, the inlet and outlet total pressure distributions were related by fractional span to compute the total pressure loss rather than following a streamline. Due to the inability of the design system to properly predict loss for this accelerating passage, the loss was assumed to be negligible during that phase of the effort. The typical CARL blade thickness distribution using cubics on each half of the blade was also used during preliminary design studies, but it was found to produce more loss than the NACA65 section in the CFD simulations.

Figure 16 shows the comparison of deviation angle for the swirler section. The throughflow method uses Carter's rule to compute deviation. The comparison shows a difference of about 2° over most of the span, excluding the endwalls.

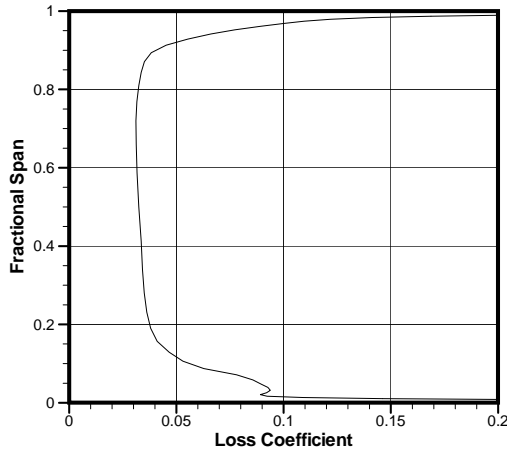


Figure 15 Swirler Vane Loss Coefficient Distribution Obtained From The CFD Simulation

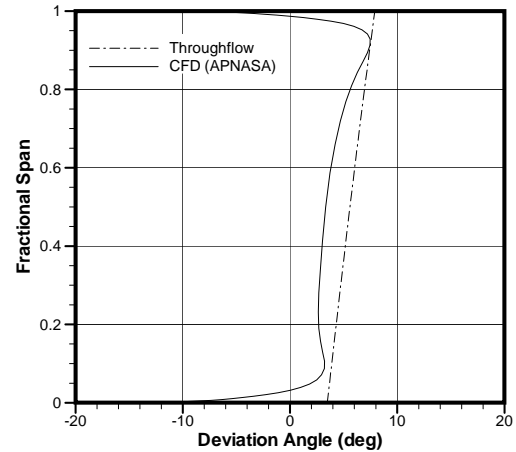


Figure 16 Swirler Vane Deviation Angle Distribution Throughflow/CFD Comparison

The near-surface flow traces are shown in Figures 17 and 18. The flow is quite well behaved. The only noticeable deviation from streamline flow is at the endwalls near the trailing edge on the suction side (Figure 17). These features result from the overturning that occurs due to the cross-passage pressure gradient that is directed from the pressure to suction sides of opposing blades within the passage.

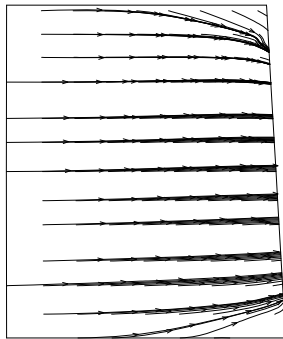


Figure 17 Swirler Vane Suction Side Near-Surface Flow Traces

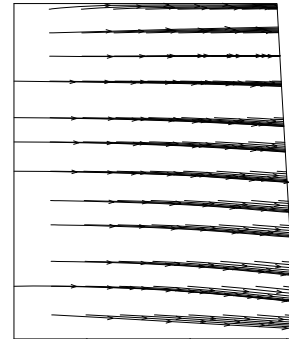


Figure 18 Swirler Vane Pressure Side Near-Surface Flow Traces

4.1.2. Stator Section

The goal for the stator section was to be representative of a well-designed, moderately loaded stator vane. It was therefore necessary that the flow be well behaved at the design point, i.e. a minimal amount of flow separation should exist so that a representative suction side boundary layer would interact with the downstream rotor flow field. Initial attempts resulted in significant corner separation at both endwalls, most pronounced at the hub. This was presumably due to the cylindrical annulus constraint. Typically, the annulus through the stator blade would contract to provide the proper axial velocity ratio for the stator row and reaction for the stage. Contraction of the hub wall produces some “free” diffusion through conservation of angular momentum due to the increasing radius. The constant hub radius through the

stator section blade row negated this potential contribution. This problem was addressed by creating an 8 mil (0.008”) gap under the hub and tip sections where it intersects the hub and tip annulus surfaces. The flow was improved dramatically as the leakage flow energized the low momentum flow in the vane/case and vane/hub corners. The disadvantage of this approach is the creation of clearance vortices and associated blockage as the flow moves downstream as shown in Figure 19. This was seen as the best compromise in terms of program objectives.

Digital Particle Image Velocimetry (DPIV) was intended to be used as the primary detailed flow field diagnostic during the program. DPIV requires optical access for both the laser light sheet source and the recording device (camera). A window was mounted in the case to provide camera access. One of the potential methods for introducing the laser light sheet was through the stator airfoil. This need constrained both the airfoil maximum thickness and its location. The laser optics required a hole along the span of the vane of 4 mm in diameter. This constraint, in combination with the requirement for pinned attachments, resulted in airfoil thickness specifications listed in Table 2 with the resulting blade shapes shown in Figure 20.

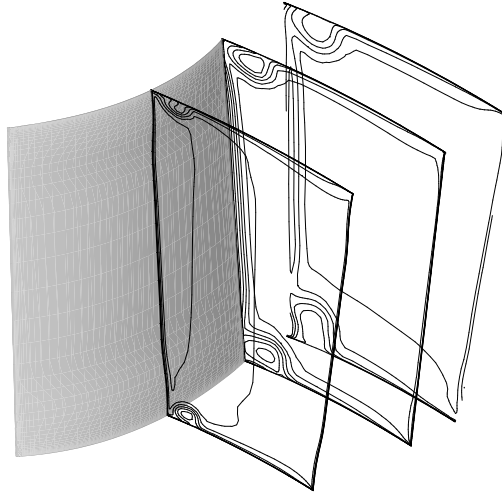


Figure 19 Stator Section Endwall Vortex Trajectories

Table 2 Stator Section Airfoil Thickness Distribution Parameters

SL#	LE Radius/Chord	TE Radius/Chord	Max T/Chord	% Chord Max T
1	0.00420	0.00420	0.100	0.400
2	0.00420	0.00420	0.100	0.412
3	0.00330	0.00330	0.080	0.425
4	0.00330	0.00330	0.080	0.437
5	0.00330	0.00330	0.080	0.449
6	0.00330	0.00330	0.080	0.462
7	0.00330	0.00330	0.080	0.474
8	0.00330	0.00330	0.080	0.486
9	0.00330	0.00330	0.080	0.498
10	0.00420	0.00420	0.100	0.510
11	0.00420	0.00420	0.100	0.523

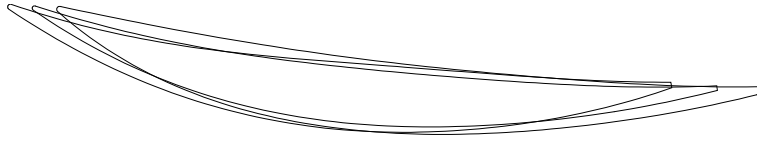


Figure 20 Stator Section Airfoil Stack (Hub, Mid, and Tip Sections)

Several 3D renderings showing views of the stator section vane is shown in Figure 21. Just as for the swirler section, the flare at the endwall to accommodate pinned attachments is evident in the frontal view (middle image).

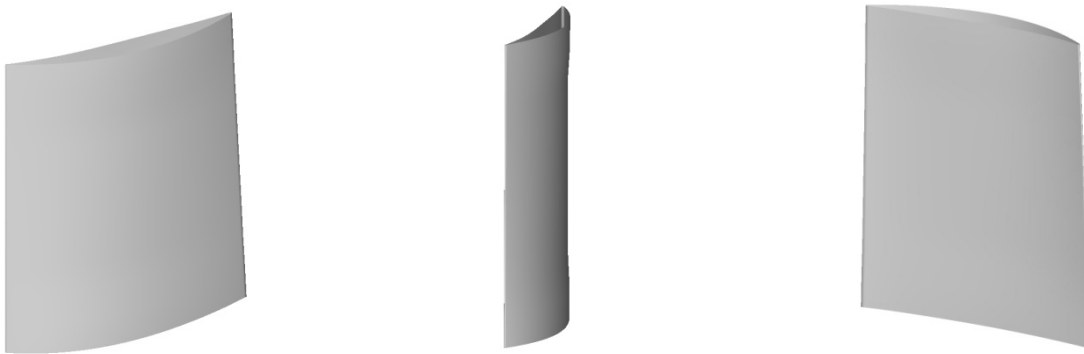


Figure 21 Multiple Views of the Stator Section Vane

The solidity of the stator vane was adjusted to achieve the Diffusion Factor goal of 0.45. In this case, the number of vanes was dictated by the need for optical access. Thirty-two vanes was necessary to provide sufficient coverage of the downstream 1/3 wake generator chord at the close spacing configuration. Therefore solidity was controlled exclusively by adjusting the axial chord of the vane. The resulting spanwise solidity distribution is shown in Figure 22. Figure 23 shows the spanwise Diffusion Factor distribution for both the throughflow and CFD results. The CFD results show a Diffusion Factor of between 0.43 and 0.44 over most of the span, with increases in the endwalls. The throughflow results show Diffusion Factors between 0.35 and 0.37. This fairly large discrepancy is due to the difference in inlet Mach number shown in Figure 24. The CFD results indicate a Mach number between 0.82 and 0.84 whereas the throughflow results are between 0.72 and 0.74. Since the trailing edge Mach numbers agree within about 0.2 Mach, the CFD solution indicates that a higher diffusion (and therefore Diffusion Factor) occurs between leading and trailing edges. Therefore the primary source of disagreement in Diffusion Factor is due to the inlet Mach number difference. The difference in Mach number can be attributed to the blockage differences between the two solutions. Blockage is specified in the throughflow method whereas an effective blockage results from the flow field calculations in the CFD solution. In the throughflow method used here, a blockage of 0.3% was specified at the stator section leading edge with 2.5% at the trailing edge. In order to match the CFD Mach number distributions, the leading edge blockage needed to be 7.5% and the trailing edge blockage needed to be 4.5%. A reduction in blockage through a diffusing passage seems unlikely. However, lacking further plausible explanation, the CFD results were taken as closer to reality and therefore the design goal was considered met. Some relief was

planned into the hardware build with the ability to vary the swirler section and therefore change the loading on the stator section.

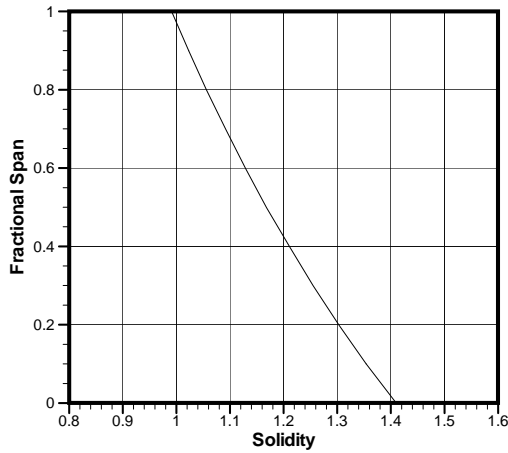


Figure 22 Spanwise Solidity Distribution for the Stator Vane Section

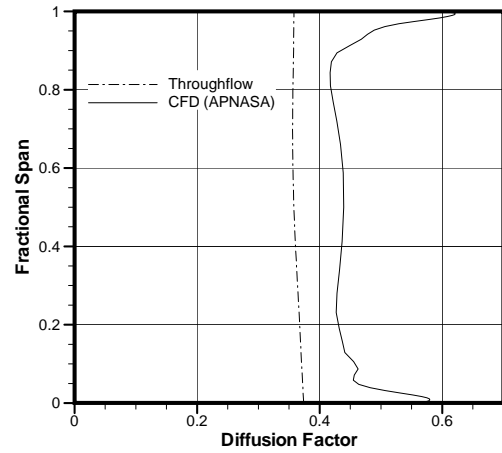


Figure 23 Spanwise Diffusion Factor Distribution for the Stator Vane Section

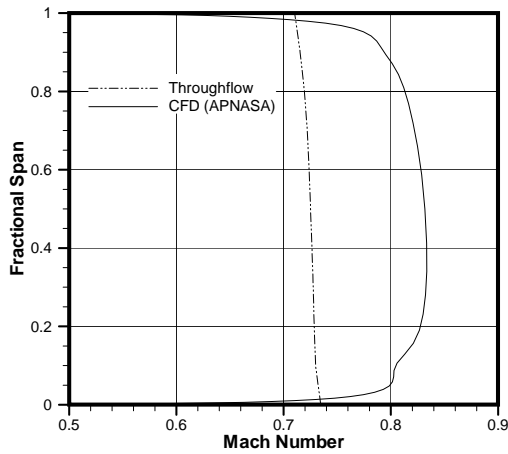


Figure 24 Stator Vane Section Inlet Mach Number Spanwise Distribution

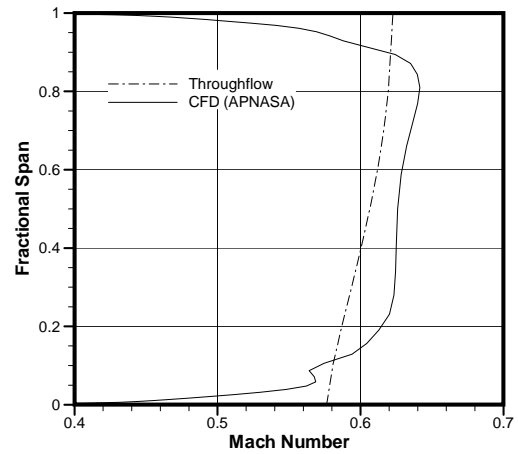


Figure 25 Stator Vane Section Exit Mach Number Spanwise Distribution

The stator incidence angle distribution is shown in Figure 26. Fairly good agreement is seen between the CFD and throughflow results with the exception of the overturning that is predicted by the CFD calculation at the endwalls. Similar behavior is also seen in the flow angle distribution shown in Figure 27 with the core flow showing excellent agreement.

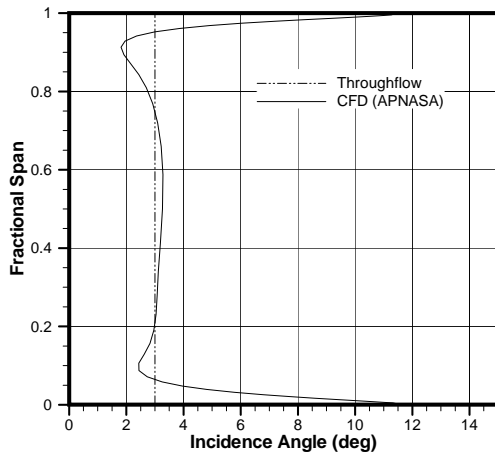


Figure 26 Stator Section Incidence Angle Spanwise Distribution

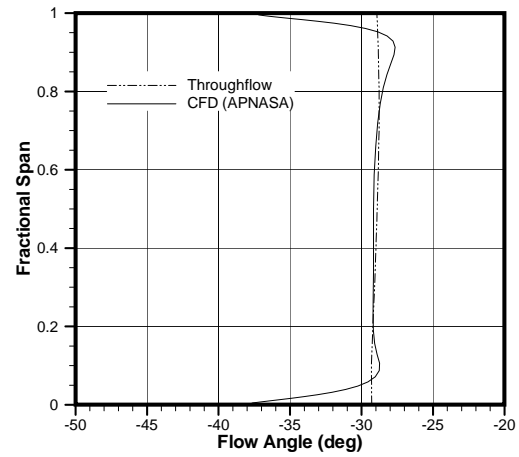


Figure 27 Stator Section Inlet Flow Angle Spanwise Distribution

The deviation and exit flow angle distributions for the stator section are shown in Figures 28 and 29, respectively. Again, endwall effects are seen in the CFD solutions while absent from the throughflow results. In Figure 29, the flow angles are precisely zero from the throughflow solution and are not readily apparent from the figure.

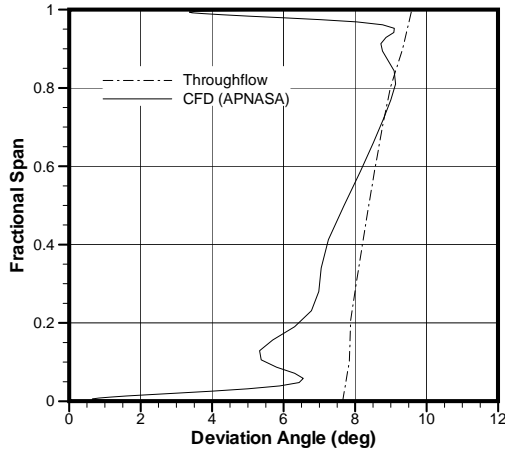


Figure 28 Stator Section Deviation Angle Spanwise Distribution

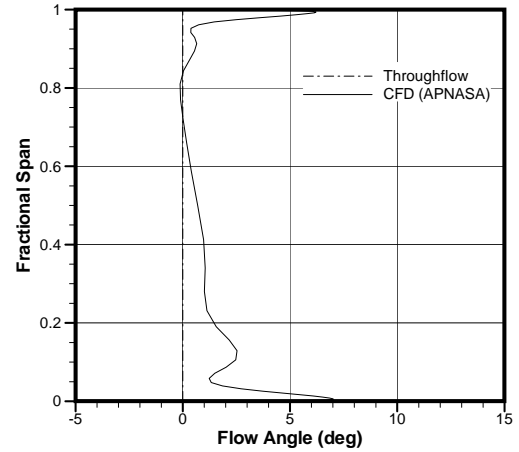


Figure 29 Stator Section Exit Flow Angle Spanwise Distribution

Figure 30 provides the spanwise loss coefficient distribution for the stator section. Relatively large loss regions are apparent in the CFD solution near the endwalls. This is presumably due to the clearance vortices. The core region is seen to be fairly low loss. This was the compromise in flow field performance struck by introducing clearance between the vane and annulus at both endwalls.

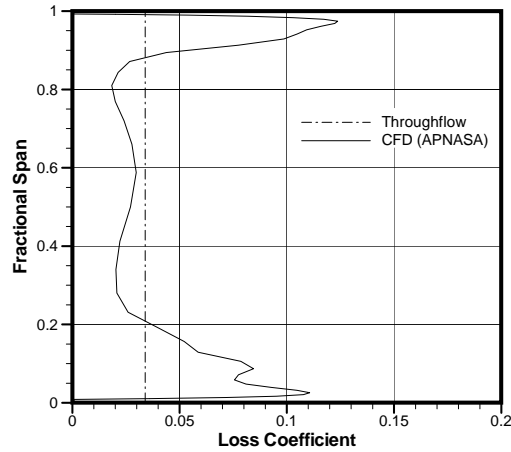


Figure 30 Stator Section Loss Coefficient Spanwise Distribution

Surface flow traces for the stator section are shown in Figures 31 and 32. Both are fairly well behaved with some minor secondary flow evident on the suction side near the trailing edge (Figure 32).

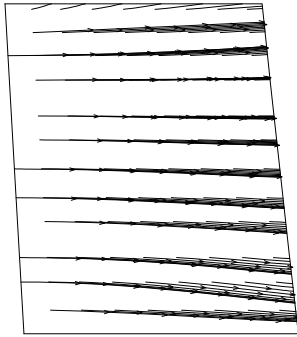


Figure 31 Stator Section Pressure Side Near-Surface Flow Traces

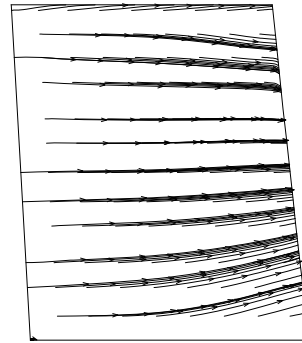


Figure 32 Stator Section Suction Side Near-Surface Flow Traces

It was intended that the flow field provided to the rotor would be as close to design conditions as possible. This involved matching flow angle and Mach number. Figures 33 and 34 shown comparisons of throughflow, CFD, and design relative flow angles and relative Mach numbers. The design values were taken from the original fan rotor design reported by Law and Wennerstrom [4]. The throughflow and CFD results all indicate a higher relative Mach number over the span which is consistent with Figure 25 which shows that the absolute Mach number at the exit of the stator section is highest for the CFD results. This difference in Mach number results from neglecting the effect of blockage in the original Law and Wennerstrom design. The effect of the increased Mach number on the rotor is to reduce its incidence angle as shown in Figure 35. While the design point flow field is not precisely reproduced, it was felt that this performance level was adequate because the difference in blockage between the design being presented here and the uncambered wake generators (Cheatham and Tyner [5]) was minimal. This would

result in proper back-to-back experimental conditions that would be comparable for the two configurations.

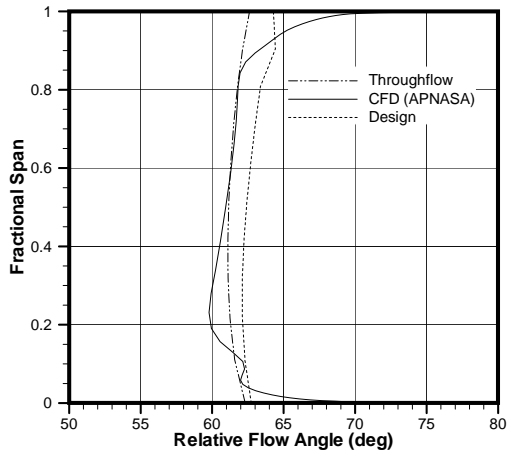


Figure 33 Rotor Relative Flow Angle Spanwise Distribution

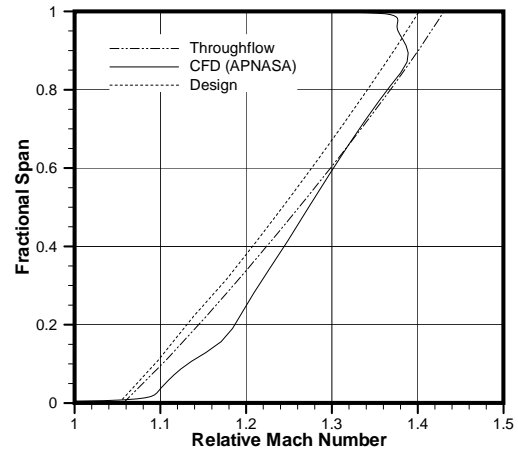


Figure 34 Rotor Relative Mach Number Spanwise Distribution

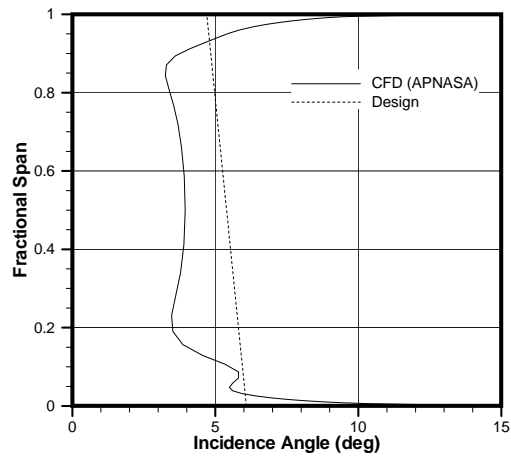


Figure 35 Rotor Incidence Angle Distribution

5. Conclusions

A 2-blade row wake generator vane set has been designed to replace an uncambered wake generator vane set to be used in a blade row interaction experimental study. The new vane set is intended to closely represent a moderately loaded stator vane that is typical of current design practice. The throughflow code UD0300M and the CFD code APNASA were used for the design work. Most of the design effort centered on the stator (downstream) section of the vane set. The primary driver for consideration of the design was to achieve a Diffusion Factor of 0.45 over the span and well-behaved flow. Despite constraints on annulus shape, axial extent of the vane set, and vane count this goal was achieved primarily through adjustment of stator chord length. Properly behaved flow was achieved at this loading level and annulus shape by introducing 8 mil gaps at the hub-vane and tip-vane endwalls in the stator section.

6. References

1. Gorrell, S.E., Okiishi, T.H., and Copenhaver, W.W., "Stator-rotor interactions in a transonic compressor - Part 1: Effect of blade-row spacing on performance," *ASME Journal of Turbomachinery*, v 125, n 2, p 328-335, April 2003.
2. Gorrell, S.E., Okiishi, T.H., and Copenhaver, W.W., "Stator-rotor interactions in a transonic compressor - Part 2: Description of a loss-producing mechanism," *ASME Journal of Turbomachinery*, v 125, n 2, p 336-345, April 2003.
3. Cumpsty, N.A., *Compressor Aerodynamics*, Longman Scientific and Technical, Essex, U.K., 1989.
4. Law, C.H. and Wennerstrom, A.J., "Two Axial Compressor Designs for a Stage Matching Investigation," AFWAL-TR-89-2005, March 1989.
5. Cheatham, J.G. and Tyner, T.M., "Stage Matching Investigation," WL-TR-91-2098, July 1991.

Appendix A

NACA65 thickness distribution applied to UD0300M.

The NACA65 thickness distribution implemented in UD0300M is based on the distribution given in Cumpsty [3] as shown in Table 3. This is a distribution originally developed for isolated airfoils that has been adapted for turbomachinery applications. Since the trailing edge thickness goes to zero at the trailing edge, a transition of the tabulated distribution to a linear profile is typically made at about 60% chord according to Cumpsty.

Table A-1 NACA 65 Thickness Distribution

% Chord	%Thickness ¹	% Thickness ²
0.161	0.442	
0.250	0.542	
0.350	0.642	
0.500	0.771	0.772
0.750	0.939	0.932
1.25	1.171	1.169
2.50	1.574	1.574
5.00	2.177	2.177
10.00	3.040	3.040
15.00	3.666	3.666
20.00	4.143	4.143
25.00	4.503	4.503
30.00	4.760	4.760
35.00	4.924	4.924
40.00	4.996	4.996
50.00	4.812	4.812
55.00	4.530	4.530
60.00	4.146	4.146
65.00	3.682	3.682
70.00	3.156	3.156
75.00	2.584	2.584
80.00	1.987	1.987
90.00	0.810	0.810
95.00	0.306	0.306
100.00	0.000	0.000

¹Modified thickness distribution used in UD0300.

²Thickness distribution given by Cumpsty (1).

The thickness distribution specified above was defined as the nominal distribution with 5% thickness-to-chord. Airfoils requiring a different thickness would be scaled from it. The modifications to this distribution detailed below are done to the nominal airfoil and then scaled to obtain the final thickness distribution.

In order to maintain compatibility with typical USAF blade thickness specifications, a leading edge radius was applied to the profile. An 80° arc was used to define the leading edge from surface to surface. The point of tangency with the surface was (0.1607,0.4416) and the center of the arc was defined as (0.687,0.0), both on the nominal thickness distribution.

Specification of the leading edge in this way required slight variation of the surface coordinates to maintain smoothness. A quadratic function was used to smooth the coordinates that resulted in an addition of 3 new points (including the tangency point) and the modification of 3 more points up to the 2.5% chord location.

Finally, the transition to a non-zero trailing edge thickness was done using a second order curve rather than a linear distribution in order to maintain slope at the transition location. If (x_0, y_0) is the transition coordinate and (x_1, y_1) is the trailing edge coordinate (y_1 being the trailing edge radius), then a curve of the form $y = Ax^2 + Bx + C$ where:

$$\begin{aligned}
 A &= \frac{S_0(x_0 - x_1) + y_1 - y_0}{(x_0 - x_1)^2} \\
 B &= S_0 - 2Ax_0 \\
 C &= y_0 - Ax_0^2 - Bx_0 \\
 \text{where } S_0 &= \left. \frac{\partial y}{\partial x} \right|_{x_0}
 \end{aligned} \tag{2}$$

LIST OF ACRONYMS, ABBREVIATIONS, AND SYMBOLS

AFRL	Air Force Research Lab
APNASA	Steady, multistage CFD code developed by NASA
CARL.....	Compressor Aero Research Lab
CFD.....	Computation Fluid Dynamics
DPIV	Digital Image Velocimetry
HIT	High Impact Technologies
\dot{m}	Mass flow rate
PIV	Particle Image Velocimetry
R_H	Hub radius
R_T	Tip radius
RZT	Turbine Engine Division
RZTF.....	Fan and Compressor Branch
S_0	tangency definition for NACA 65 surface definition
SMI	Stage Matching Investigation
UD0300M	Streamline curvature axial compressor design code developed by USAF
V	Velocity
x_0	x coordinate of the transition point in the NACA 65 surface definition
x_1	x coordinate of the trailed edge in the NACA 65 surface definition
y_0	y coordinate of the transition point in the NACA 65 surface definition
y_1	y coordinate of the trailed edge in the NACA 65 surface definition
α	Absolute flow angle
ρ	Density